

LOW DIMENSIONAL MODELS FROM LARGE DATASETS OF COMPLEX FLOWS USING FULL ORTHOGONALIZATION ARNOLDI DYNAMIC MODE DECOMPOSITION

Sreevatsa Anantharamu

Aerospace Engineering and Mechanics
University of Minnesota
110 Union St. SE, Minneapolis, USA
anant035@umn.edu

Praveen Kumar

Aerospace Engineering and Mechanics
University of Minnesota
110 Union St. SE, Minneapolis, USA
prave002@umn.edu

Krishnan Mahesh

Aerospace Engineering and Mechanics
University of Minnesota
110 Union St. SE, Minneapolis, USA
kmahesh@umn.edu

ABSTRACT

Dynamic Mode Decomposition (DMD) is being used in recent years to analyze and derive low order models of complex systems including fluid flows. Anantharamu & Mahesh (2019) proposed a novel DMD algorithm suitable for analysis of large datasets, which is used here to analyze the complex flow field of a reverse rotating propeller attached to hull. The datasets employed in the present work are obtained from the large eddy simulation results of Verma *et al.* (2012). The employed DMD algorithm is well-suited for such large datasets due to its memory and computational efficiency, and better accuracy, compared to other popular streaming DMD algorithms. The DMD spectra for both datasets show dominant peaks consistent with the previously reported force spectra. The corresponding DMD modes are analyzed for their relevance to overall dynamics.

INTRODUCTION

Dynamic mode decomposition (DMD) (Schmid, 2010; Rowley *et al.*, 2009) is an attractive tool to study complex physical as it isolates the regions associated with a particular frequency through the computed DMD modes and eigenvalue. Each DMD mode has its own amplitude signifying its contribution to the overall system dynamics. Since it was first proposed, there are numerous variations of the original method available in literature, each with its own merits and demerits depending on the problem at hand. The key idea of DMD is to approximate eigenvectors and eigenvalues of the unknown system matrix from the snapshots matrix. Each of the DMD modes has an assigned eigenvalue that gives its temporal growth/decay rate along with its frequency. The readers are referred to the reviews by Mezić (2013) and Rowley & Dawson (2017) for detailed information about these methods.

Most of the popular DMD methods are not efficient in handling large datasets typically obtained in any high-

fidelity simulation. Moreover, the accuracy of the extracted modes and eigenvalues are usually unknown for a given number of snapshots. To overcome these shortcomings, (Anantharamu & Mahesh, 2019) proposed a DMD algorithm suitable for large datasets. The algorithm is parallel and streaming with low memory requirement and computational cost. Additionally, the algorithm provides error indicator for each of the DMD mode and eigenvalue pairs. Owing to the dependency of DMD on the snapshot vectors, it was discussed the finite precision errors can be detrimental if the condition number of the snapshot matrix is large. Also, different DMD algorithms which are theoretically identical can lead to different results. For snapshot matrices with large condition number, FOA based DMD has an optional rank truncation step to reduce errors in the computed modes without losing its streaming property. A detailed analysis of the computational cost and memory requirement of FOA based DMD can be found in Anantharamu & Mahesh (2019).

Verma *et al.* (2012) performed LES of flow over propeller attached to hull in crashback, which is an off-design operating condition where the flow due to propeller rotation is opposite to the incoming freestream. Crashback condition is characterized by massive flow separation and large propeller loads due to formation of a ring vortex as shown in Figure 1. They simulated crashback flow over a marine propeller (DTMB P4381) with and without an axisymmetric hull (DTMB 5495-3) at a Reynolds number $Re_D = 480000$ for two advance ratios $J = -1$ and $J = -0.5$. Here $J = \frac{U}{nD}$ and $Re = \frac{UD}{\nu}$, where U is the freestream velocity, n is the propeller rotation rate, ν is the kinematic viscosity and D is the propeller diameter. Their simulations reproduced the experimentally observed behaviour of high side force in the presence of hull at higher negative advance ratio (Bridges, 2004). Based on their results, they proposed a mechanism to explain this behaviour.

In this paper, the datasets of Verma *et al.* (2012) are used to perform DMD. The simulation details of Verma

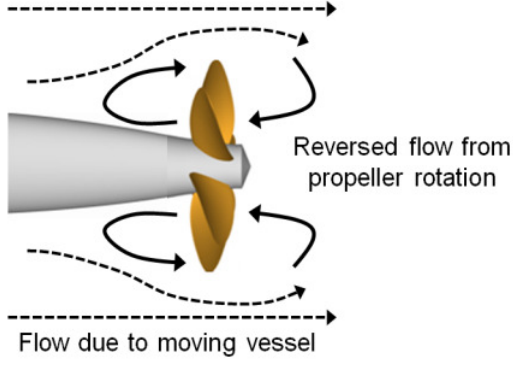


Figure 1: Schematic of flow over propeller in crashback.

et al. (2012) are briefly summarized in the next section, followed by an overview of the DMD algorithm of Anantharamu & Mahesh (2019). Finally, the DMD results are discussed in detail, followed by a brief summary of the present work.

SIMULATION DETAILS

In LES, large scales are resolved by the spatially filtered Navier–Stokes equations, whereas the effect of small scales is modelled. Simulations are performed in a frame of reference that rotates with the propeller. The spatially filtered incompressible Navier–Stokes equations in the rotating frame of reference are formulated for the absolute velocity vector in the inertial frame as follows:

$$\begin{aligned} \frac{\partial \bar{u}_i}{\partial t} + \frac{\partial}{\partial x_j} (\bar{u}_i \bar{u}_j - \bar{u}_i \varepsilon_{jkl} \omega_k x_l) = \\ - \frac{\partial \bar{p}}{\partial x_i} - \varepsilon_{ijk} \omega_j \bar{u}_k + \nu \frac{\partial^2 \bar{u}_i}{\partial x_j \partial x_j} - \frac{\partial \tau_{ij}}{\partial x_j} \quad (1) \\ \frac{\partial \bar{u}_i}{\partial x_i} = 0 \end{aligned}$$

where u_i is the inertial velocity in the inertial frame, p is the pressure, x_i are coordinates in the rotating non-inertial reference frame, ω_j is the angular velocity of the rotating frame of reference, ν is the kinematic viscosity, ε_{ijk} denotes the permutation tensor and the approximation $\bar{u}_i \varepsilon_{jkl} \bar{\omega}_k x_l \approx \bar{u}_i \varepsilon_{jkl} \omega_k x_l$ is used. The terms containing ω_j in the eq. 2.1 take into account the effect of rotating reference frame which is non-inertial. $\frac{\partial}{\partial x_j} (-\bar{u}_i \varepsilon_{jkl} \omega_k x_l)$ represents Coriolis acceleration whereas $-\varepsilon_{ijk} \omega_j \bar{u}_k$ is representative of centrifugal acceleration. The overbar $(\bar{\cdot})$ denotes the spatial filter and $\tau_{ij} = \bar{u}_i \bar{u}_j - \bar{u}_i \bar{u}_j$ is the sub-grid stress. The sub-grid stress is modelled by the Dynamic Smagorinsky Model (Germano *et al.*, 1991; Lilly, 1992). The Lagrangian time scale is dynamically computed based on surrogate-correlation of the Germano–identity error (Park & Mahesh, 2009). This approach extended to unstructured grids has shown good performance for a variety of cases including flow past a marine propeller in crashback (Verma & Mahesh, 2012).

Eq. 1 is solved by a numerical method developed by Mahesh *et al.* (2004) for incompressible flows on unstructured grids. The algorithm is derived to be robust without

any numerical dissipation. It is a finite volume method where the Cartesian velocities and pressure are stored at the centroids of the cells and the face normal velocities are stored independently at the centroids of the faces. A predictor–corrector approach is used. The predicted velocities at the control volume centroids are first obtained and then interpolated to obtain the face normal velocities. The predicted face normal velocity is projected so that the continuity equation in eq. 1 is discretely satisfied. This yields a Poisson equation for pressure which is solved iteratively using a multigrid approach. The pressure field is used to update the Cartesian control volume velocities using a least-square formulation. Time advancement is performed using an implicit Crank–Nicholson scheme. The algorithm has been validated for a variety of problems over a range of Reynolds numbers (see Mahesh *et al.*, 2004).

FOA based DMD

Let M and N be the size and the number of snapshots used to perform DMD. Assuming A to be the linear mapping between two successive snapshots, FOA based DMD generates the set of Arnoldi vectors $\{v_i\}_{i=1}^N$ and the matrix $\bar{H}_N \in \mathbb{C}^{N \times (N-1)}$ that are related to A as

$$\begin{aligned} AV_1^{N-1} &= V_1^N \bar{H}_N, \\ AV_1^{N-1} &= V_1^{N-1} H_{N-1} + h_{N,N-1} v_N e_{N-1}^H, \end{aligned} \quad (2)$$

where $v_i \in \mathbb{C}^M$, $V_1^{N-1} \in \mathbb{C}^{M \times (N-1)}$ is the matrix formed by stacking the vectors $\{v_i\}_{i=1}^{N-1}$ as columns, H_{N-1} is the upper Hessenberg matrix and is the leftmost $(N-1) \times (N-1)$ portion of \bar{H}_N , e_{N-1}^H is the transpose of the canonical basis vector $e_{N-1} \in \mathbb{C}^{N-1}$, $h_{N,N-1}$ is the $(N, N-1)^{th}$ entry of the matrix \bar{H}_N . Also, H_{N-1} is the projection of the linear mapping A onto the range of V_1^{N-1} . The DMD modes and eigenvalues are $\{V_1^{N-1} z_i\}_{i=1}^{N-1}$ and $\{\lambda_i\}_{i=1}^{N-1}$ respectively, where $\{\lambda_i, z_i\}_{i=1}^{N-1}$ are the eigenvalue and eigenvector pair of the projected linear mapping H_{N-1} .

In the present work, we use the batch processed form of FOA based DMD without rank truncation described in algorithm 1 to compute the DMD modes and eigenvalues. The computation was performed using 192 processors and the orthonormal matrix V_1^{N-1} and the upper Hessenberg matrix \bar{H}_N are computed. The DMD modes for each J were computed in an hour on Knights Landing cluster at the Texas Advanced Computing Center. The matrix of snapshots are loaded into memory and are overwritten by the orthonormal matrix V_1^{N-1} thereby efficiently utilizing the available memory.

Next, we review the auxiliary tools of FOA based DMD method for analysis of the computed DMD modes. The coefficient vector $\{c\} \in \mathbb{C}^{N-1}$ of the first vector ψ_1 when represented as a linear combination of the DMD modes can be obtained by solving the $(N-1) \times (N-1)$ matrix problem,

$$\{c\} = \|\psi_1\|_2 [z]^{-1} e_1, \quad (3)$$

where $[z]$ is the matrix formed by stacking the vectors z_1 to z_{N-1} as columns and e_1 is the first canonical basis vector of

- 1: Collect N snapshots and form X_1^N .
- 2: Construct initial vector v_1 from the first snapshot,
 $v_1 := \frac{\psi_1}{\|\psi_1\|_2}$.
- 3: $\beta_{1,1} = \|\psi_1\|_2$
- 4: **for** $j=1$ to $N-1$ **do**
- 5: $\beta_{1,j+1} = h_{1,1:j-1} \beta_{1:j-1,j}$
- 6: **for** $i=2$ to j **do**
- 7: $\beta_{i,j+1} = h_{i,i-1:j-1} \beta_{i-1:j-1,j}$
- 8: **end for**
- 9: $w = \frac{1}{\beta_{j,j}} (\psi_{j+1} - \sum_{i=1}^j \beta_{i,j+1} v_i)$
- 10: $h_{1:j,j} = V_1^{jH} w$
- 11: $w = w - V_1^j h_{1:j,j}$
- 12: $s_{1:j} = V_1^{jH} w$
- 13: $h_{1:j,j} = h_{1:j,j} + s_{1:j}$
- 14: $w = w - V_1^j s_{1:j}$
- 15: $h_{j+1,j} = \|w\|_2; v_{j+1} = \frac{w}{h_{j+1,j}}$
- 16: **for** $i=1$ to $j+1$ **do**
- 17: $\beta_{i,j+1} = \beta_{i,j+1} + h_{i,j} \beta_{j,j}$
- 18: **end for**
- 19: **end for**
- 20: Define $H_{N-1} := \bar{H}_N(1:N-1, 1:N-1)$.
- 21: Compute right eigenvectors $\{z_i\}_{i=1}^{N-1}$ and eigenvalues $\{\lambda_i\}_{i=1}^{N-1}$ of H_{N-1} .
- 22: DMD modes are $\{V_1^{N-1} z_i\}_{i=1}^{N-1}$ and DMD eigenvalues are $\{\lambda_i\}_{i=1}^{N-1}$.

Algorithm 1: FOA based DMD in batch processed form without rank truncation.

\mathbb{C}^{N-1} . We then have,

$$\psi_1 = \sum_{i=1}^{N-1} c_i \varphi_i, \quad (4)$$

where c_i is the i^{th} entry of $\{c\}$ and the DMD mode $\varphi_i := V_1^{N-1} z_i$. The coefficient of all the snapshot vectors $\{\psi_i\}_{i=1}^{N-1}$ as a linear combination of DMD modes $\{\varphi_i\}_{i=1}^{N-1}$ can then be obtained as

$$\psi_i = \sum_{j=1}^{N-1} c_j \lambda_j^{i-1} \varphi_j; i = 1, \dots, N-1. \quad (5)$$

From the above expression we can define the spectra for DMD modes corresponding to the i^{th} snapshot as the set of numbers $\{[c_j \lambda_j^{i-1}]\}_{j=1}^{N-1}$.

The residual of each DMD mode and the eigenvalue can be computed. This residual serves as the error indicator for the accuracy of the corresponding mode and eigenvalue due to the error resulting from Galerkin projection. The residual of i^{th} DMD mode is computed as

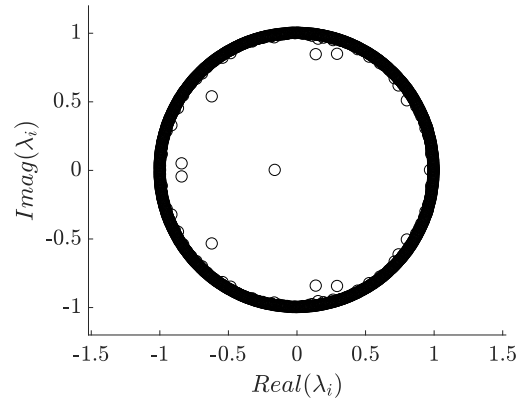
$$\|AV_1^{N-1} z_i - \lambda_i V_1^{N-1} z_i\|_2 = h_{N,N-1} \|e_{N-1}^H z_i\| \quad (6)$$

RESULTS

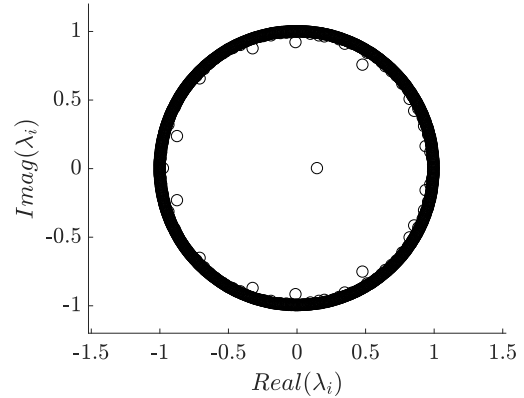
The velocity vector at each control volume in the grid is chosen to be the vector of observables. The set of observable vectors is denoted as $\{\psi_i\}_{i=1}^N$ where $\psi_i \in \mathbb{R}^M$, M is the size of the observable vector ψ_i and N is the number of snapshots. We define X_1^j as a matrix $\in \mathbb{R}^{M \times (j-i+1)}$ formed

by the stacking the vectors ψ_i to ψ_j as columns. For both the cases, $N = 1200$ and $M \approx 21.9 \times 10^6$ i.e. three times the number of control volumes in the grid. The dataset for both the advance ratio cases comprises 1200 snapshots spanning $T = 60$ rotations of the propeller with a sampling rate . i.e. $\Delta t = 0.05$ rotation time.

The 2-norm condition number $\kappa_2(X_1^{N-1})$ for $J = -0.5$ and -1 cases is approximately 104 and 110 respectively. Since, $\kappa_2 \ll 1/\epsilon_m$, rank truncation is not needed to compute the DMD modes and eigenvalues. The normalized DMD frequency $f := \log(\lambda)/(2\pi\Delta t)$. The imaginary part of f will be called as the oscillation frequency of the corresponding mode.



(a) $J = -0.5$



(b) $J = -1$

Figure 2: DMD eigenvalues.

Figure 2 shows the DMD eigenvalues for both the cases. Most of the eigenvalues lie on the unit circle. The DMD spectra showing the magnitude of component of the projection of the last snapshot along each of the DMD eigenvectors are plotted in figure 3. The peak at $f \approx 0$ denotes the time-averaged flow field. The spectra show dominant peaks at integral value of f for both the cases. Recall that the frequency is normalized to be unity at the shaft frequency. Table 1 and 2 shows the frequencies of the first five dominant DMD modes for $J = -0.5$ based on the spectra of the last snapshot along with the associated residual. The error indicator (residual) suggests that the modes are converged to accurate values and addition of more snapshots would not change the results significantly.

Table 1: Residual of the DMD modes sorted based on DMD spectra of last snapshot for $J = -0.5$.

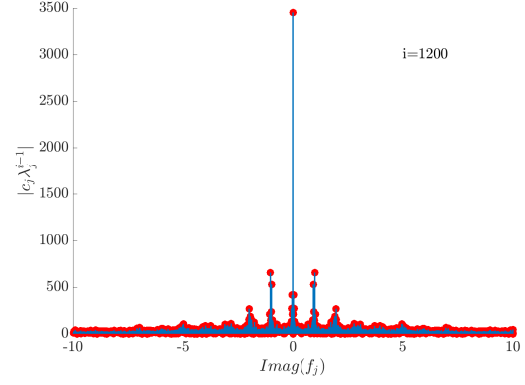
f	Residual
$-2.5e-5$	$9e-4$
$9.5e-4 + 1.0i$	$6.3e-3$
$2.2e-4 + 9.7e-1i$	$8.4e-3$
$-4.3e-4 + 3.6e-2i$	$9.8e-3$
$-2.6e-3 + 5.5e-2i$	$1e-2$

Table 2: Residual of the DMD modes sorted based on DMD spectra of last snapshot for $J = -1$.

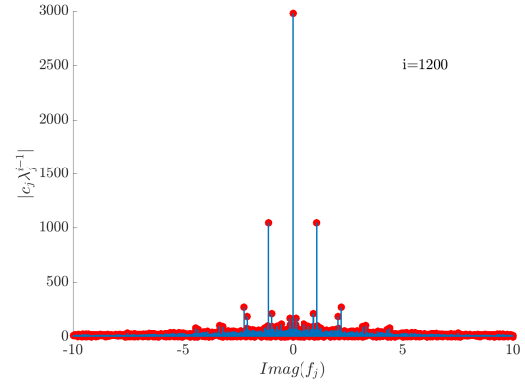
f	Residual
$7e-5$	$1.7e-3$
$1.3e-4 + 1.12i$	$2.6e-3$
$1.6e-4 + 2.23e-1i$	$0.9e-2$
$-3.9e-4 + 0.97i$	$1.03e-2$
$-1.5e-3 + 2.08e-2i$	$1.33e-2$

DMD modes with the smallest real and imaginary part are shown in figure 4 for both the cases. A slice facing downstream through the propeller blade with contour plot of the x-component of the DMD modes is shown. These correspond to the mean flow for both the cases. We can see that the regions in the vicinity of the blade have reverse flow in the mean when compared with the free stream velocity.

In figure 5, we show a side view of the iso-surface of the streamwise (x) component of the real part of the dominant DMD mode with imaginary part of frequency $f \approx 1$. The translucent slice is colored with the same quantity. Figure 5(b) is further elucidated in figure 6 by plotting stream-traces that pass through the plotted isosurfaces. The stream-traces close to the blade show that these modes correspond to the vortex shedding mode. The vortices are formed due to the interaction of the reverse flow due to the propeller with the freestream. Once the vortex is shed near the propeller blade, they undergo swirling motion due to the propeller rotation as seen from figure 6. It can be seen that for $J = -0.5$ the mode has a significant component in the region upstream of the propeller on the hull whereas for $J = -1$ it is dominant only in the downstream of the propeller. This is because of the stronger reverse flow in $J = -0.5$ than in $J = -1$. Also, for $J = -1$ the modes are wrapped around closer to the blade than for $J = -0.5$ which qualitatively indicates closer location of the vortex to the propeller blade. This is consistent with the observation in LES of Verma *et al.* (2012). Since, the propeller has 5 blades, DMD modes that oscillate with frequency approximately 1 (i.e. $im(f) \approx 1$) leads to a peak at $f \approx 5$ in the integrated side force spectra of the propeller blade. This is because the approximate azimuthal wavenumber of the mode is also 1. Hence, the propeller sees a similar configuration of the flow (but rotated) for every $(1/5)^{th}$ rotation of the propeller



(a) $J = -0.5$



(b) $J = -1$

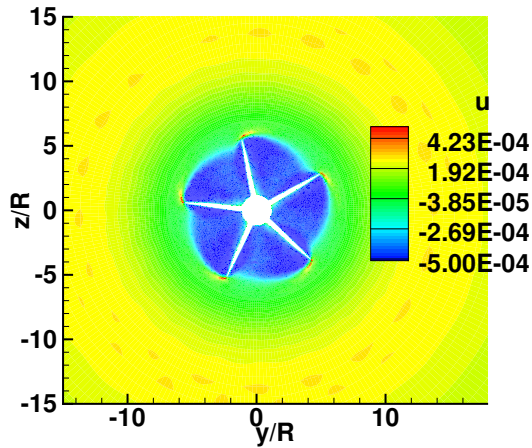
Figure 3: DMD spectra for the last snapshot.

blade thus explaining the peak at 5 in the force spectra of the propeller.

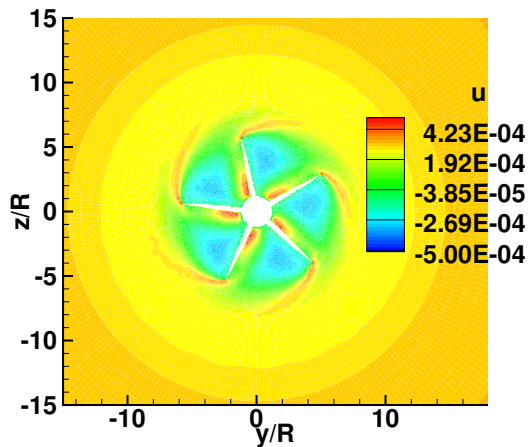
Figure 7 shows the x-component of the real part of the dominant DMD modes oscillating with frequency ≈ 2 . The azimuthal wavenumber of these modes is seen to be ≈ 2 . These modes contribute to the force spectra of the propeller blade at frequencies $f \approx 10$. The presence of higher harmonics of the fundamental shedding frequency is similar to that seen in the DMD modes obtained for the snapshots comprising vortex shedding behind circular cylinders. It is interesting to observe similar behavior in the complex flow configuration of a propeller in crashback mode.

CONCLUSION

We have performed DMD of the dataset of propeller in crashback mode at $J = -0.5$ and $J = -1$ using the recently proposed parallel FOA based DMD algorithm proposed suitable for large datasets. The algorithm helps pick out the dominant DMD mode and also the error in each mode due to Galerkin projection. The two dominant DMD modes for both cases are seen to be associated with the vortex shedding due to the interaction of the reverse flow of the propeller with the freestream with imaginary part of the frequency ≈ 1 and 2 which contribute to the force spectra of the propeller at ≈ 5 and 10 respectively. The mode shapes are qualitatively seen to be consistent with the previous LES of Verma *et al.* (2012). These dominant mode shapes form a low-dimensional set of basis vectors which help build a reduced order model for a high Reynolds number flow field of propeller in crashback mode.



(a) $J = -0.5$



(b) $J = -1$

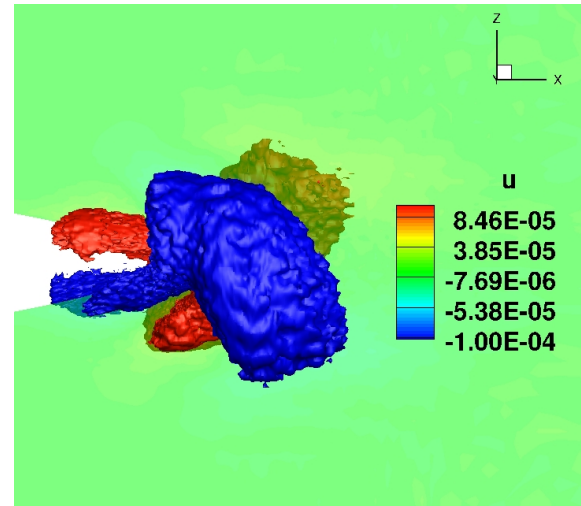
Figure 4: The DMD mode at $f = -2.5 \times 10^{-5}$ for $J = -0.5$ (top) and (b) $f = 7 \times 10^{-5}$ for $J = -1$ (bottom).

ACKNOWLEDGEMENT

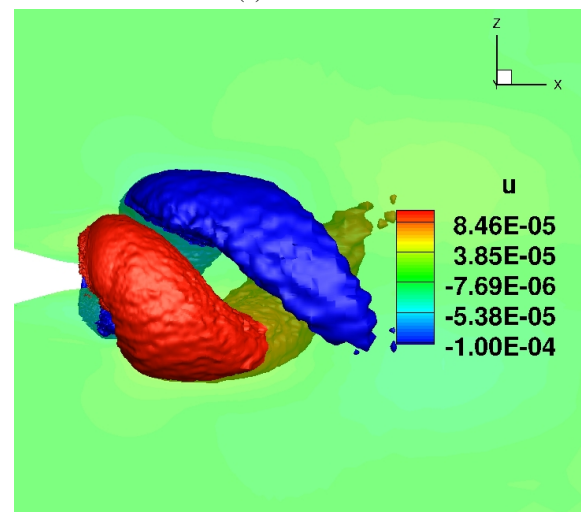
This work was supported by the United States Office of Naval Research under ONR Grant N00014-18-1-2356 with Dr. Ki-Han Kim as technical monitor. Computing resources were provided by the Extreme Science and Engineering Discovery Environment (XSEDE) allocation and the Minnesota Supercomputing Institute.

REFERENCES

- Anantharamu, S. & Mahesh, K. 2019 A parallel and streaming dynamic mode decomposition algorithm with finite precision error analysis for large data. *Journal of Computational Physics* **380**, 355–377.
- Bridges, D. H. 2004 A detailed study of the flowfield of a submarine propeller during a crashback maneuver. *Tech. Rep. MSSU-ASE-04-1*. Department of Aerospace Engineering, Mississippi State University.
- Germano, M., Piomelli, U., Moin, P. & Cabot, W. H. 1991 A dynamic subgrid-scale eddy viscosity model. *Physics of Fluids A* **3**:7, 1760.
- Lilly, D. K. 1992 A proposed modification of the Germano



(a) $J = -0.5$



(b) $J = -1$

Figure 5: The DMD modes at $f = 0.9 \times 10^{-3} + 1.02i$ for $J = -0.5$ (top) and $f = 0.1 \times 10^{-3} + 1.12i$ for $J = -1$ (bottom) are shown for streamwise velocity along with the isosurface of streamwise velocity with values $\pm 10^{-3}$.

subgrid-scale closure model. *Physics of Fluids A* **4**:3, 633.

- Mahesh, K., Constantinescu, G. & Moin, P. 2004 A numerical method for large-eddy simulation in complex geometries. *Journal of Computational Physics* **197** (1), 215–240.
- Mezić, I. 2013 Analysis of fluid flows via spectral properties of the koopman operator. *Annual Review of Fluid Mechanics* **45**, 357–378.
- Park, N. & Mahesh, K. 2009 Reduction of the Germano-identity error in the dynamic Smagorinsky model. *Physics of Fluids (1994-present)* **21** (6), 065106.
- Rowley, C. W. & Dawson, S. T. M. 2017 Model reduction for flow analysis and control. *Annual Review of Fluid Mechanics* **49**, 387–417.
- Rowley, C. W., Mezić, I., Bagheri, S., Schlatter, P. & Henningson, D. S. 2009 Spectral analysis of nonlinear flows. *Journal of Fluid Mechanics* **641**, 115–127.
- Schmid, Peter J 2010 Dynamic mode decomposition of nu-

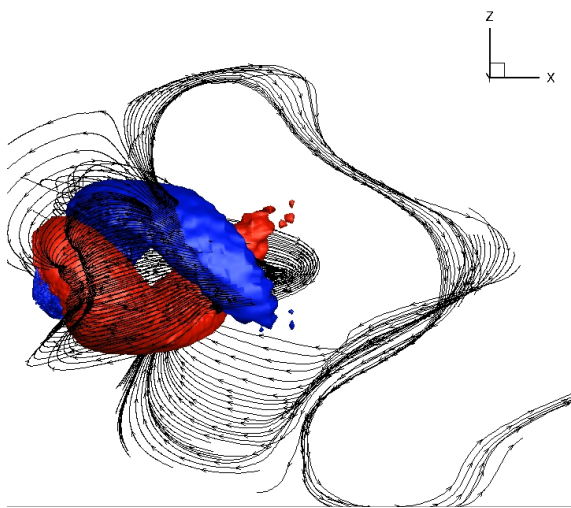
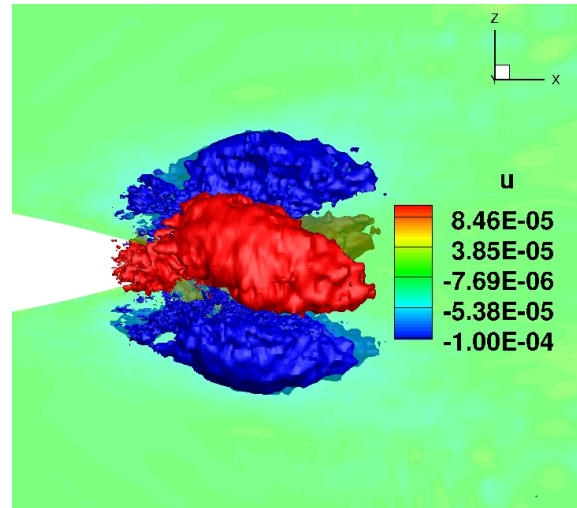
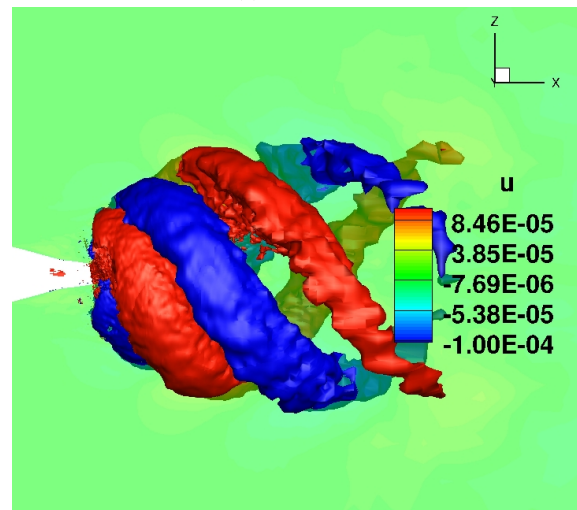


Figure 6: Flow structures in figure 5(b) elucidated using streamtraces.



(a) $J = -0.5$



(b) $J = -1$

merical and experimental data. *Journal of Fluid Mechanics* **656**, 5–28.

Verma, A., Jang, H. & Mahesh, K. 2012 The effect of an upstream hull on a propeller in reverse rotation. *Journal of Fluid Mechanics* **704**, 61–88.

Verma, A. & Mahesh, K. 2012 A Lagrangian subgrid-scale model with dynamic estimation of Lagrangian time scale for large eddy simulation of complex flows. *Physics of Fluids (1994-present)* **24** (8), 085101.

Figure 7: The DMD modes at (a) $-1 \times 10^{-4} + 1.99i$ for $J = -0.5$ (top) and $f = 1.3 \times 10^{-4} + 2.3i$ for $J = -1$ (bottom) are shown for streamwise velocity along with the isosurface of streamwise velocity with values $\pm 2 \times 10^{-3}$.